Desalination and Water Treatment
www.deswater.com
doi: 10.5004/dwt.2020.24738

173 (2020) 351–366
January

Comparison between dead anaerobic biomass and synthesized Fe_3O_4 nanoparticles for the removal of Pb(II), Ni(II) and Cd(II)

Farouk Abdullah Rasheed[a,*], Shahlaa Esmail Ebrahim[b]

[a]*Civil-Environmental Engineering Department, University of Sulaimani, Iraq, Tel. +9647702174301; email: Farouk.rasheed@univsl.edu.iq*
[b]*Environmental Engineering Department, University of Baghdad, Iraq, Tel. +9647707947617; email: shahlaa.ebrahim@fulbrightmail.org*

Received 14 March 2019; Accepted 26 July 2019

ABSTRACT

Dead anaerobic biomass and synthesized Fe_3O_4 were used to remove lead, nickel and cadmium metal ions. In the single element system, the maximum uptake of Pb(II), Ni(II) and Cd(II) ions, respectively on the biomass was favorably 59.48, 17.74 and 32.8 mg g^{-1} at pH 4 for 4 h contact time compared to 31.5, 4.36 and 20.56 mg g^{-1} at pH 6 for an hour of equilibrium time when using the synthesized Fe_3O_4. Langmuir's model corresponded well with experimental anaerobic adsorbent data while Freundlich presented the best matching for nanosorbent data. Thermodynamic investigation revealed that the adsorption process on both adsorbents was exothermic and physically occurred. Only biomass was conducted in the binary and ternary process to show the metallic competition to occupy the vacant sites on the biomass surface and then evaluate adsorption isotherm constants for each adsorption model. In the single and multiple metal systems, lead ions had a high affinity to stick with both adsorbents opposed to nickel and cadmium ions. The adsorption capacities order for the metals were: Pb(II) > Cd(II) > Ni(II). The resulted data from the kinetic process have good compliance with the pseudo-second-order model. Fluidization of biomass was adopted to show breakthrough curves of metals under the effect of different operating conditions and experimental data fitted well with the predicted data obtained by applying artificial neural network.

Keywords: Dead anaerobic biomass; Fe_3O_4 nanoparticles; Heavy metals; Comparison; ANN

1. Introduction

Over the past few decades, rapid urbanization and widespread industrialization have inevitably resulted in an increased concentration of several hazardous pollutants in unmanageable wastewater discharge, which directly influences the quality of biotic resources due to severe toxicity and carcinogenic property of pollutants [1,2]. Therefore, environmental legislative standards have become stricter. Heavy metals are considered to be threatening pollutants which are both hazardous and toxic. They are known as non-biodegradable contaminants, which remain in water sources in the environment and through a bioaccumulation process, increase their quantity in plant and aquatic tissue, thus having an antagonistic influence on human being's health once transferred into the food chain [3]. The metals which are the greatest environmental issue are lead, nickel and cadmium [4]. According to World Health Organization standards, the permissible limit of these three metals in drinking water is 0.05, 0.2 and 0.01 mg L^{-1}, respectively. The presence of lead in drinking water with low concentration may cause anemia, hepatitis and nephritic syndrome. The toxic level in humans causes severe damage to the kidney, nervous system, reproductive system, liver and brain [5]. High intake or inhalation of nickel causes genotoxic in cell culture systems, DNA damage, chromosomal damage and weak mutagenicity in mammalian cells [6]. Cadmium waste streams from the industries can pollute both soil

* Corresponding author.

and water. The organic matter in the soil absorbs cadmium increasing the risk of survival of various plants and also increases the uptake of the toxic metals in food. The most severe form of Cd(II) toxicity in humans is 'itai-itai' [7]. Therefore, the removal of these toxic contaminants is crucial prior to their release into the environment [8,9] by effectively and simply treating contaminated water [10].

The instantaneous removal of these toxic pollutants from wastewater is a noticeable issue in the aerobic and aquatic world. Several physical and chemical methodologies have been developed to control these toxic contaminants successfully such as, chemical method, filtration, membrane separation, electrochemical treatment and ion exchange. All of the above methods are costly, with high energy input, large quantities of chemical reagents being required, having high chemical sludge production and demonstrating inefficient low-level metal contamination removal from wastewater [11]. Therefore, cost effective alternative technologies for the treatment of metal-contaminated waste streams are needed [12].

Adsorption is considered as a preferred method owing to its high pollutant removal efficiency, low required cost, high flexibility, reusability and selectivity for specific metal, simplicity of design and operation, and insensitivity to toxic pollutants [13,14]. Due to its large surface area, high adsorption capacity and surface reactivity, adsorption using activated carbon are able to adsorb various metal ions from inorganic water effluent. However, the use of activated carbon might be unsuitable for developing countries due to its expensive cost [15]. In recent years, alternative low-cost adsorbents that have binding capacities have attracted the attention of several investigators for providing alternative treatments. Various waste materials and microorganism have been reported as biosorbents such as agricultural waste, industrial by-products, natural materials or modified polymer for the removal of metal ions [16,17]. A number of microbial biosorbents like bacteria, fungi, yeast and cyanobacteria have been studied for the removal of toxic metals from waste streams [18]. A significant amount of waste sludge is produced in industrial and municipal wastewater treatment plants daily, disposal of which is one of the biggest environmental problems in the world. Thus, stabilization through anaerobic digestion and utilization are a preferred solution for sludge management [19]. On the other hand, currently, nano-sized metal oxides, including nano-sized ferric oxides, manganese oxides, aluminum oxides, titanium oxides, magnesium oxides and cerium oxides are classified as 'promising adsorbents' for heavy metal removal from aqueous systems [20]. Iron oxide Fe_3O_4 nanosized particles are widespread in nature, have the structure of an inverse spinel and differ from most other iron oxides in that they contain both Fe(II) and Fe(III). Co-precipitation is the most widely used method for the synthesis of nanoparticles of controlled sizes [21,22]. The production and application of iron oxide nanoparticles in the laboratory with low cost in comparison with commercial ones (acquired from Houston nanoparticle research in USA, TX 77084) were attractive to modify and employ as nanosorbent in adsorbing of Pb(II), Ni(II) and Cd(II) ions. Even though the performance and effectiveness of synthesized Fe_3O_4 nanoparticles are not totally equivalent to the commercial ones, the function of synthesized Fe_3O_4 is preferable and feasible to remove the three metal ions. Furthermore, the application of low cost and highly efficient of dead anaerobic biomass has been also developed and utilized to remove the same metal ions from wastewater because generation piles of anaerobic sludge daily makes not only environmental problems, but also creates restrictions in disposal sites. In this study, both dead anaerobic biosorbent and laboratory synthesized Fe_3O_4 nanosorbent prepared with the lowest cost compared with commercial ones were examined to show their viability and effectiveness to adsorb lead, nickel and cadmium ions in single component system. The adsorbent which demonstrated the optimum performance would be taken as the preferable adsorbent to be used in multiple, kinetic, and continuous systems. Characterization of both adsorbents was also tested using techniques of X-ray fluorescence (XRF), transmission electron microscopy (TEM) and Fourier transfer infrared (FTIR) to show their different properties.

2. Materials and methods

2.1. Metal solutions

Chemical reagent powders of $Pb(NO_3)_2$, $Ni(NO_3)_2{\cdot}6H_2O$ and $Cd(NO_3)_2$ (BDH/England-purity 99.5%) were used to prepare (1,000 mg L^{-1}) a stock metal solution for each of lead, nickel and cadmium ions. Quantities of 1.6, 4.953 and 2.104 g of lead nitrate, nickel nitrate and cadmium nitrate respectively, were weighed and mixed with 200 mL of deionized water and a volume of 10 mL of concentrated nitric acid. Once a uniform metal solution was reached, Dilution was applied by the further addition of deionized water up to 1,000 mL [23]. The desired normality was obtained after diluting a limited volume of concentrated solution with deionized water. Dissolved metal concentrations in solution were measured by an inductively coupled plasma optical emission spectrometer (ICPOES) (Optima 2100DV, PerkinElmer Inc., UK).

2.2. Dead anaerobic biosorbent

A sample of live biomass, including heterogeneous microorganisms (bacteria, yeast, and fungi) was drawn by a suction pump from 3 m depth of the concrete thickener of the wastewater treatment plant that continuously supplied by biosolids, pumped from the bottom of the secondary sedimentation tank. According to the history of this plant, the precipitated biomass in the concrete thickener was accumulated and left for more than a year; therefore, the sample was taken to the drying and measuring the particle diameter before the growing step of the microbial content in the sample. Fortunately, the resulted diameter was 1.1 mm more than the optimal needed in the experimental work, for this reason; there was no need to increase the biomass particle diameter through using the nutrient medium. The biomass was dried at atmospheric temperature (37°C–45°C) for 5 d, then passed through sieves of 500 and 900 μm mesh size. The average mean diameter is given as $d_{am} = (d_1 d_2)^{1/2}$ where d_1 denotes the inferior sieve diameter in which biomass granules are retained, while d_2 represents the upper sieve diameter which allows particles to pass through it [24].

The solid biomass was washed thoroughly with deionized water to confirm that no foreign impurities were attached to the biomass prior to its use in these experiments, and then oven dried for 2 d at 70°C to remove its moisture content.

2.3. Iron oxide nanoparticle preparation in laboratory

The amount of 5.4 g ferric chloride hexahydrate ($FeCl_3 \cdot 6H_2O$) and 3.6 g of technical urea $(NH_2)_2CO$ (purity 99%, total nitrogen content 46%, Prilled urea, Shandong factory, China) were weighed and mixed in a conical flask using 200 mL distilled water. A water bath was turned on and set on 90°C to heat the mixture until the color of the solution turned from clear orange to khaki. The liquid mixture was left for a while to cool down and then a magnetic stirrer with a speed of 600 rpm was used to mix the solution with an additional 2 g of ferrous chloride tetrahydrate ($FeCl_2 \cdot 4H_2O$) for 15 min. Some drops of NaOH solution with molarity (2 mol L^{-1}) were gradually added until the pH value of the solution rose to above 10. Thus, a greenish precipitate was observed and poured into a plastic can with 500 mL capacity. Distilled water was added to fill the can and then sealed to prevent air from entering. Finally, the plastic container was abandoned at room temperature for 7 h. The precipitated black color was filtrated using Whatman filter paper No. 42, followed by washing with 500 mL of distilled water initially and then 100 mL of acetone later. The residue precipitate on the filter paper was oven-dried at 50°C for 7 h [25]. The main physical properties of both adsorbents are shown in Table 1. To identify the chemical composition which formulated the structure of both adsorbents, the XRF (Spectro IQ11/ Ametek, materials analysis division/Germany) technique scan was used. The results are illustrated in Table 2 showing that the oxides of SiO_2, CaO and Al_2O_3 in the biosorbent hold the highest composition percentage which are (12.58%, 4.53% and 3.82%), respectively while for synthesized nanosorbent, Fe_2O_3 takes the largest quantity in its composition (54.84%). The functional bands attributed to those oxides in both adsorbents give better attraction properties for enhancing the adsorption of metal contaminants from bulk liquid.

2.4. TEM image analysis

TEM scan has its strong points of interest as it appropriates direct pictures and local information on morphology, distribution and stage present of particles. The micrographs in Fig. 1 provide information about size, shape and distribution of particles for both of biosorbent and synthesized Fe_3O_4 nanoparticles. The biosorbent exhibited a rough surface providing a large vacant area for metal ion interaction [26]. The images also demonstrate that small pores are existed on the biosorbent surface whereas no pore sizes are noticeable in the nanosorbent images. The existence of pore sizes on the surface of biosorbent is helpful for further uptake of solute pollutants from the bulk solution and enhances deeply intraparticle diffusion [26].

2.5. Evaluation of optimum pH

The pH value of the metal solution is essential to proceed with adsorption because it changes the adsorbent surface charge, degree of ionization and speciation of pollutant species [27]. To find the best pH value demonstrating maximum efficiency to remove metal ions, the following procedure was followed:

The amount of 0.05 g of each adsorbent (biomass or nanosorbent) was added separately to six volumetric flasks, each containing 100 mL of a single heavy metal solution with a concentration of 40 mg L^{-1} for Pb(II), Ni(II) and Cd(II) ions, respectively. The pH value of the solutions in the six flasks was adjusted from 3–8 using 0.1 M sodium hydroxide or nitric acid solution with an agitation speed of 200 rpm for a period of 4 h for biosorbent and 60 min for nanosorbent at a laboratory temperature of 20°C. Finally, samples of 10 mL from each volumetric flask were taken, filtered and measured in concentration by (ICPOES).

Table 1
Main physical properties of dead anaerobic biomass and synthesized Fe_3O_4 nanosorbent

Properties	Anaerobic biomass	Fe_3O_4 nanosorbent
Purity	Not determined	±97%
Average particle size	0.5–0.9 mm	50–80 nm
Surface area (m^2 g^{-1})	92.93	55.23
Color dark	Black	Clear brown
Morphology	Irregular	Spherical
Bulk density (g cm^{-3})	0.59	0.79
True density (g cm^{-3})	1.513	4.73

Table 2
Chemical Properties of anaerobic biomass and synthesized iron oxide nanosorbent Fe_3O_4

Compounds	Anaerobic biomass	Fe_3O_4 nanosorbent
$\%Fe_2O_3$	1.73	54.85
$\%SiO_2$	12.58	0.113>
$\%Al_2O_3$	3.821	0.203
$\%TiO_2$	0.2676	0.0064
%MnO	0.0146	0.2
%MgO	2.836	0.26
%Cl	0.0368	1.71
%CaO	4.526	0.011
$\%P_2O_5$	1.905	0.017
$\%SO_3$	1.546	0.002

2.6. Equilibrium contact time

A quantity of 0.5 g of each adsorbent (anaerobic biomass and Fe_3O_4 nanosorbent) was blended separately with 100 mL of single metal ion solutions in a number of hipflasks of 250 mL capacity with a concentration of 40 mg L^{-1} Pb(II), Ni(II), and Cd(II) ions. The solutions were adjusted to pH 4 for biomass and six for nanosorbent, at an agitation speed of 200 rpm. Samples with a volume of 10 mL were taken at each period and their metal ion concentration measured using (ICPOES).

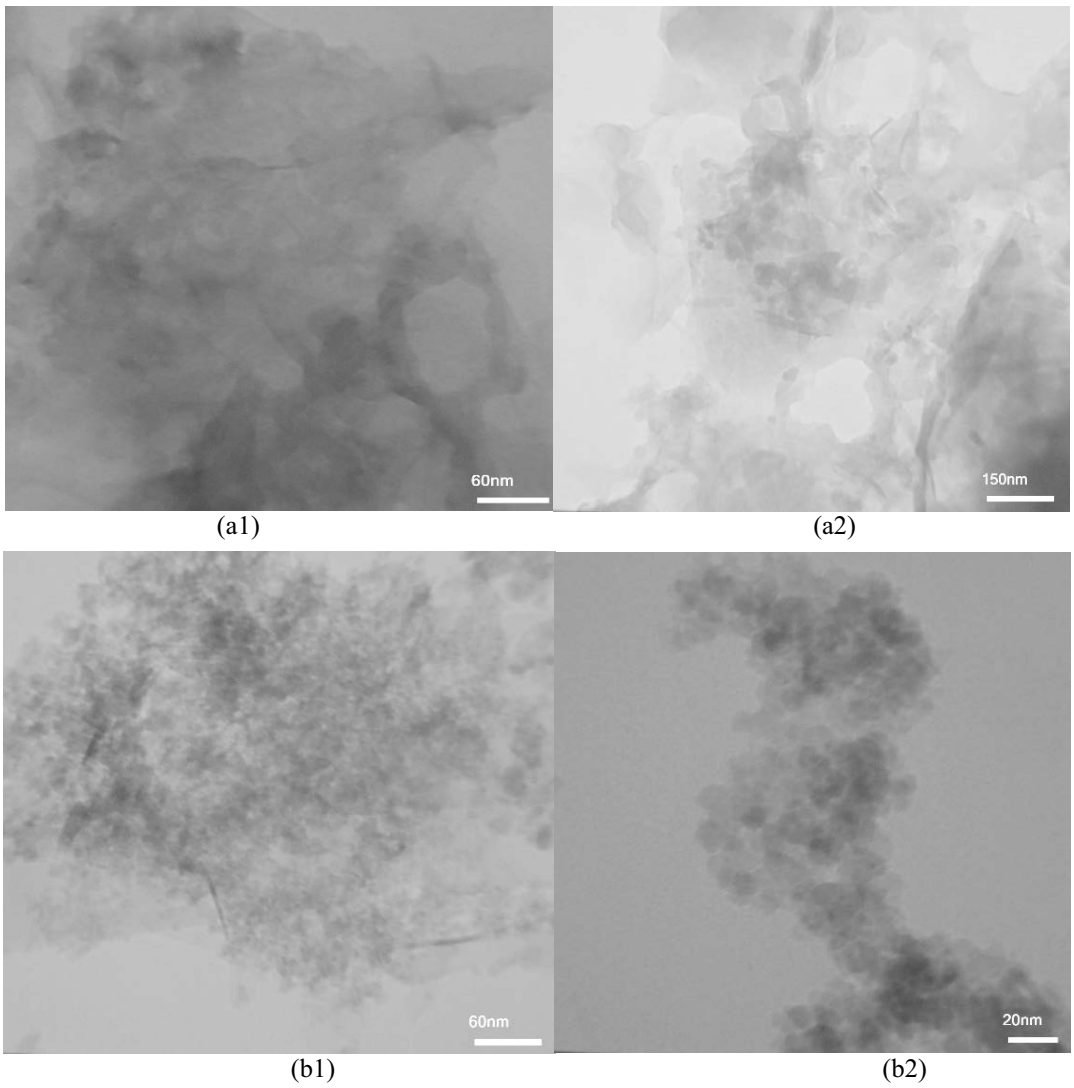

Fig. 1. Transmission electronic micrographs for (a1,a2) dead anaerobic biomass and (b1,b2) synthesized Fe_3O_4 nanoparticles.

2.7. Isothermal equilibrium experimentations

2.7.1. Single module system

Various masses of the dry dead biomass 0.05, 0.1, 0.15, 0.2, 0.25, 0.3, 0.35, 0.4, 0.5 and 0.6 g were distributed into 10 volumetric hipflasks of 250 mL. Solutions with a concentration of 40 mg L^{-1} were prepared for single systems of lead, nickel and cadmium ions respectively and 100 mL from each solution was added to each hipflask. The pH value of solutions in the flasks was fixed to the desired value using 0.1 M sodium hydroxide or nitric acid. A thermoshaker was used to agitate continuously for up to 4 h at a speed of 200 rpm and at a temperature of 20°C. Each sample was filtered through Whatman filter paper (No. 1) and a few droplets of the nitric acid were added to lower its pH value below 2 prior to analysis [23]. In the case of Fe_3O_4 nanoparticle, the quantity of nanosorbent used was 0.05, 0.1, 0.15, 0.2, 0.4, 0.6, 0.8, 1, 1.2 and 1.4 g and the pH value of solutions in the flasks was adjusted to six for an hour of contact time. The final equilibrium concentrations were measured by (ICPOES). The uptake q_e of the adsorbed metal ion was then calculated using the following formula [28]:

$$q_e = \frac{V_1\left(C_0 - C_e\right)}{W} \tag{1}$$

where C_0 and C_e are the initial and equilibrium metal concentrations in the experiment solution respectively and V_1 is the metal solution volume in the hipflasks and w is the dosage of biomass. Isothermal adsorption curves for each metal ion were plotted based on the amount of adsorbed solute for each unit of weighed biomass/nanosorbent (q_e) vs. the final equilibrium concentration of metal ions in the solution (C_e). The experimental laboratory data obtained from isothermal adsorption experiments was interrelated to two common non-linear adsorption model equations (Langmuir and Freundlich) through the use of statistical software-version.8 to compute fundamental parameters of each model [29].

2.8. Kinetic experiments

The adsorbent type which was more feasible and effective to adsorb the metal pollutants, applied in a kinetic process to predict the best mixing speed in order to achieve 95% removal of metal ions and identify proper kinetic adsorption model to represent the experimental data. Kinetic process investigations were managed in a Pyrex glass beaker with a 2 L capacity. 1 L of metal aqueous solution with a concentration of 40 mg L^{-1} was placed in the beaker and its pH value adjusted to 4. An impeller with 4-bladed stainless-steel axial flow was fixed at the center of the beaker cell. Agitation of the impeller was started at a speed of 200 rpm at 20°C. At the time interval zero, the accurate weight of biosorbent was added. Samples from the beaker were taken at different time intervals. These samples were filtered and then analyzed for their final equilibrium heavy metal content. The above procedure was repeated at speeds of 300, 400 and 500 rpm, then the concentration time decay curves were obtained by plotting the C_e/C_0 vs. time.

2.8.1. Adsorption kinetics models

2.8.1.1. Pseudo-first-order kinetic model

Lagergren equation is reliable to express this model. It explains the process of kinetic biosorption of the three heavy metal ions on dead anaerobic biomass [30]. The model can be denoted in the following equation [31]:

$$\frac{dq}{dt} = k_1\left(q_e - q_t\right) \tag{2}$$

where q_t and q_e (mg g^{-1}) are adsorbed to solute quantity at any time t (min) and equilibrium, respectively. k_1 (min^{-1}) is the rate constant of the pseudo-first-order. Taking integration of Eq. (2) depending on the boundary conditions of $q_t = 0$ at $t = 0$ and $q_t = q_t$ at $t = t$, the equation becomes [32]:

$$\log\left(\frac{q_{\text{eq}}}{\left(q_e - q_t\right)}\right) = \frac{k_1 t}{2.303} \tag{3}$$

Slope (k_1/2.303) and intercept (log q_e) can be attained from a plotting graph of log ($q_e - q_t$) against t. Eventually, the equilibrium metal solute uptake (q_e) and first order kinetic constant (k_1) can be acquired.

2.8.1.2. Pseudo-second-order kinetic model

The following equation is used to represent pseudo-second-order model. The mass transfer of driving force of, ($q_e - q_t$), proportionate to availability of vacant sites as shown below [33]:

$$\frac{dq}{dt} = k_2\left(q_e - q_t\right)^2 \tag{4}$$

Taking integration of Eq. (4) whilst considering boundary conditions of $q_t = 0$ at $t = 0$ and $q_t = q_t$ at $t = t$, the equation converts to:

$$\frac{1}{\left(q_e - q_t\right)} = \frac{1}{q_e} + k_2 t \tag{5}$$

where k_2 is rate constant of second order. Eq. (5) can be reorganized to demonstrate a linear relation:

$$\frac{t}{q_t} = \left(\frac{1}{k_2 q_e^2} + \frac{t}{q_e}\right) \tag{6}$$

Slope ($1/q_e$) and intercept $1/(k_2 q_e^2)$ are found from the relationship between t/q_t against t. Ultimately, the quantity of adsorbed metal per mass of biomass at the final equilibrium point (q_e) and second order rate constant (k_2) are calculated.

2.8.1.3. Intraparticle diffusion model

The biosorption process usually occurs through three various stages: (a) external surface diffusion, (b) internal surface diffusion and (c) biosorption phenomenon between the adsorbate and vacant sites on the biomass. This model is hypothesized as a controlling rate and characterized by the following formula [34]:

$$q_t = k_{\text{id}} t^{0.5} + C \tag{7}$$

where k_{id} is the rate constant for the intraparticle diffusion in (mg g^{-1} $min^{-0.5}$). The relationship between q_t against $t^{0.5}$ illustrates diffusion of solute pollutant through intraparticle. The slope gives the rate constant (k_{id}) of mass transfer coefficient through biomass intraparticle, while the intercept shows the boundary layer impact.

2.8.1.4. Elovich model

Elovich model denotes the kinetic process of chemisorption. It was discovered by Zeldowitsch in 1934 and applied to confirm the biosorption rate of adsorbate contaminants on the biomass that down trended exponentially with progress in the quantity of solute adsorbed [35]. The Elovich formula is stated as follows:

$$\frac{dq}{dt} = a\exp\left(-b\, q_t\right) \tag{8}$$

where q_t indicates the magnitude of solute biosorbed at time t, b is the desorption rate constant and a is the initial biosorption rate. Eq. (8) can be reorganized into a linear relation:

$$q_t = \left(\frac{1}{b}\right)\ln\left(t + t_0\right) - \left(\frac{1}{b}\right)\ln t_0 \tag{9}$$

Through integration and using boundary conditions $q_t = 0$ at $t = 0$ and $q_t = q_t$ at $t = t$, Eq. (9) becomes:

$$q_t = \left(\frac{1}{b}\right)\ln\left(ab\right) + \left(\frac{1}{b}\right)\ln t \tag{10}$$

The plot graph relationship of q_t against ln(t) provides slope as $\left(\frac{1}{b}\right)$ and intercept as $\left(\frac{1}{b}\right)\ln\left(ab\right)$.

2.9. FTIR analysis

Identification of types of efficient groups (carbonyl, carboxylic, hydroxyl and others) on the external surfaces of anaerobic biosorbent/Fe_3O_4 nanosorbent, requires FTIR investigation. This technique was performed on both dried biomass and Fe_3O_4 nanosorbent samples in the wave range of 4,000–400 cm^{-1} with a resolution of 4 cm^{-1}. A volumetric flask of 250 mL capacity was filled with 100 mL of metal solution (40 mg L^{-1}) and adjusted to pH value 4. Around 0.5 g mass of well-dried biomass was added to the flask, which was subsequently placed on a shaker and agitated continuously for 4 h at 200 rpm. Later, the solution was filtered. The precipitated adsorbent was collected and dried in an oven at 50°C for 24 h dried adsorbent samples (before and after being loaded with metal ions) were labelled and sent to an analytical laboratory for FTIR testing. For nanosorbent, around 0.5 g mass of unprocessed iron oxide nanoparticles was taken and dried in an oven at 50°C for 24 h. The sample was placed in a tube test, covered well, labelled and sent to an analytical laboratory for FTIR testing.

2.10. Continuous experiments

The fluidized bed adsorber studies were carried out in a glass column of 4.5 cm I.D. and 100 cm in height, a distributor and sieve with a small mesh were used at the bottom for uniform fluidizing and bearing particles in the column, while the influent solution was introduced to the column through a plastic pipe from the bottom. The schematic diagram of this experimental equipment is shown in Fig. 2. Once the hydrodynamic parameter (minimum fluidized velocity U_{mf}) was computed, column experiments were carried out to notify the breakthrough curve for the three heavy metals. Continuous tests were investigated at different static bed heights (4.1 cm–50 g, 6.1 cm–75 g and 9.2 cm–100 g) with two distinctive flow rate conditions (26.4 and 33.6 L h^{-1}, corresponding to 1.1 U_{mf} and 1.4 U_{mf}) with biomass bed particle diameters: (0.5–0.9 mm).

3. Results and discussion

3.1. Influence of pH value

Fig. 3 demonstrates that the adsorption of both adsorbents was improved significantly with an increase in pH value and achieved maximum uptake in pH 4 and 6 at 20°C for the biomass and synthesized iron oxide nanosorbent, respectively. This can be explained because the surface of the samples contains some active sites which become positively charged at low pH values [36]. Beyond the value of pH 6, precipitation will occur to solute ions due to insoluble metal hydroxides, which then start precipitating from the solutions at higher pH values and make the true sorption studies impossible. This should be avoided during sorption experiments which distinguish between sorption and precipitation [37]. Therefore, the optimum pH values of 6 and 4 were chosen and used in all subsequent experiments. Fig. 3 also reveals that lead ions have the highest tendency to become adsorbed on both adsorbents while nickel has the least affinity to do so due to the presence of various electrical attractions between cation lead metal and negative adsorption functional sites. Additionally, lead ion possesses the smallest hydration radius while nickel ion possesses the greatest, causing nickel to be less favored by both biomass and nanosorbent. This corresponds with the conception that ions with a small hydration radius are desirably selected and gathered at the interface [38,39]. Furthermore, lead nitrate salt is less soluble in water than salts of nickel and cadmium. Therefore, lead ions have the highest adsorption rate. These results are in compliance with results obtained by Ebrahim et al. [40] or Kakaei and Kazemeini [41]. Although anaerobic biomass is a waste product resulting from municipal wastewater treatment, it has effective and energetic functionality to remove metal ions. The biosorbent not only gives better performance than synthesized Fe_3O_4 nanoparticles but also exhibits environmental improvement in reducing piles of sludge after capturing metal ions and used as inorganic fertilizer in the agricultural fields.

3.2. Influence of equilibrium contact time

It was observed in Fig. 4 that the removal efficiency of the three metal pollutants by both adsorbents increased with increasing contact time. For the biosorbent, the adsorption process was rapid during the first 2 h. However, no significant increase in the sorption rate was found after 3 h and metal concentration decreased rapidly during the first 2 h and remained nearly constant after 3 h of adsorption, suggesting that the biosorption is fast and reaches saturation within 4 h. In the case of Fe_3O_4 nanosorbent, rapid adsorption occurred in the first 30 min and achieved equilibrium within 60 min. The figure revealed that lead ions have the highest tendency to be absorbed because of their nanosized granular and high surface area in which all vacant space is quickly occupied by metal ions which transfer solutes from bulk liquid to the surface of nanosorbent.

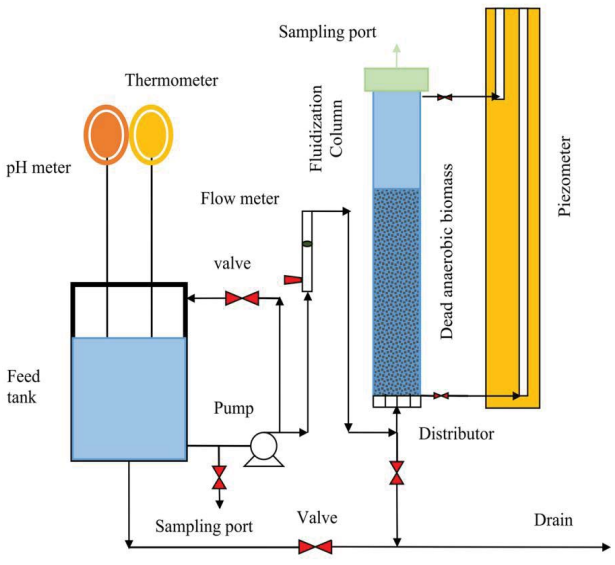

Fig. 2. Schematic diagram of fluidization of dead anaerobic biomass bed in continuous system.

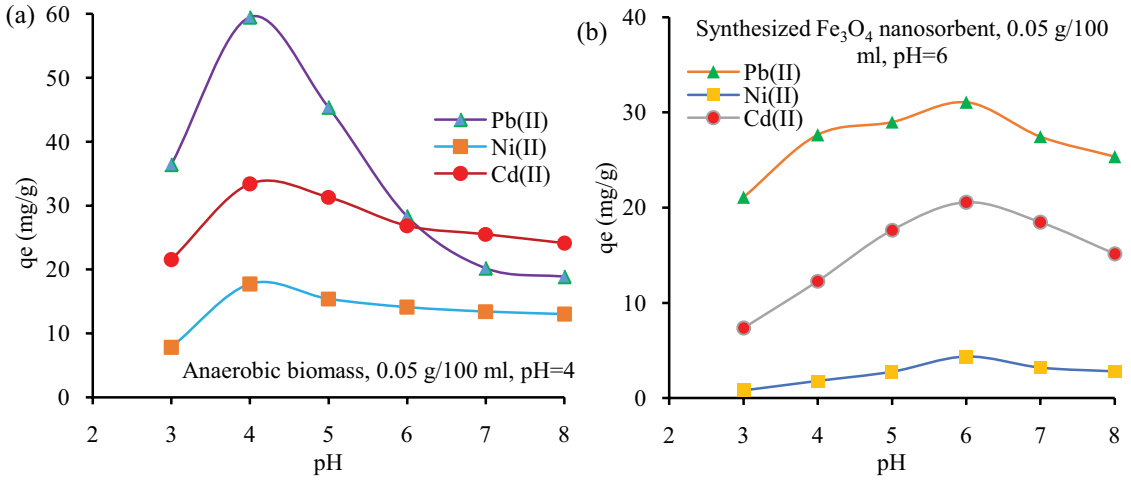

Fig. 3. Effect of different pH on lead, nickel and cadmium uptake at C_0 = 40 mg L^{-1} by (a) dead anaerobic biomass and (b) synthesized Fe_3O_4 nanosorbent.

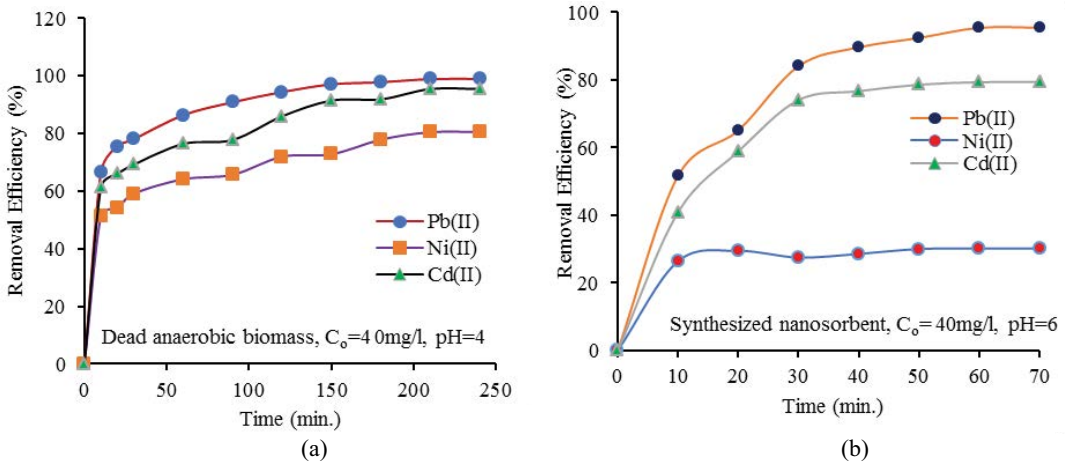

Fig. 4. Effect of contact time on the three-metal ion uptake by (a) dead anaerobic biomass and (b) synthesized Fe_3O_4 nanosorbent.

3.3. Single component module

Fig. 5 verifies the single metal uptake system by both adsorbents in solutions with concentrations of 40 mg L^{-1} at 20°C. The maximum adsorption uptakes for anaerobic biosorbents were 59.48, 17.74 and 32.8 mg g^{-1} for lead, nickel and cadmium while for the Fe_3O_4 nanosorbent, uptakes were 31.5, 4.36 and 20.56 mg g^{-1}, respectively. The maximum metal removal efficiencies achieved with 0.6 g/100 mL of dead biomass are 98.98%, 83.23% and 96.43%. However, in state of using nanosorbent form, an additional dosage of up to (1.4 g/100 mL) was needed to attain removal efficiencies of 99.7%, 65.5% and 95.07% for lead, nickel and cadmium ions, respectively. The resulting data for a single element system was interrelated with common isothermal models (Langmuir and Freundlich). Statistica software-version.8 was used to determine fundamental parameters for each model as shown in Table 3.

The research illustrated that Langmuir isothermal model was best suited for experimental data related to lead, nickel and cadmium ion adsorption onto anaerobic biosorbent while Freundlich's model was well interrelated the equilibrium data which resulted from the adsorption of the three metals on the iron oxide nanosorbent. In addition, it was found that lead ion was the most attractive pollutant as opposed to nickel and cadmium ions. This may be related to its characteristics in aqueous solutions where it demonstrates poor solubility and high molecular weight [40]. Thus, adsorption capacities for metal ion solutes follow the subsequent order: Pb(II) > Cd(II) > Ni(II). Overall, the results this in single element system predict the ability of dead anaerobic biosorbent to attract metals was noticeably more effective than synthesized Fe_3O_4 nanoparticles.

3.4. Thermodynamic parameters

To estimate the effect of temperature on adsorption of Pb(II) onto both dead anaerobic biomass and synthesized Fe_3O_4, changes in three thermodynamic parameters were evaluated: Gibbs free energy change ($\Delta G°$) in (kJ mol^{-1}) was calculated using Eqs. (11) and (12):

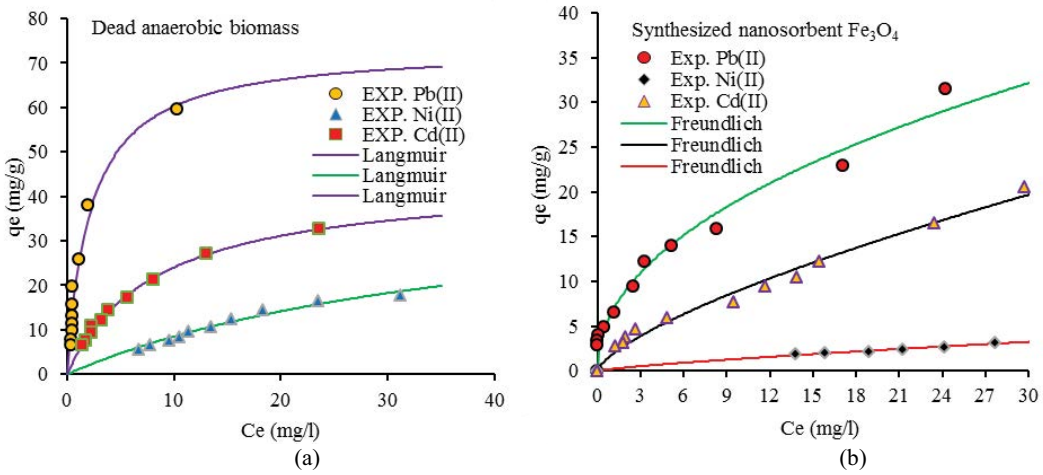

Fig. 5. Adsorption isotherms of lead, nickel and cadmium ions in a single solute system with C_0 = 40 mg L^{-1} onto (a) dead anaerobic biomass and (b) synthesized Fe_3O_4 nanosorbent.

Table 3
Parameters of single solute isotherm for Pb(II), Ni(II) and Cd(II) ions for dead anaerobic biomass and Fe_3O_4 nanosorbent

Model	Parameter	Anaerobic biomass			Fe_3O_4 nanosorbent		
		Pb(II)	Ni(II)	Cd(II)	Pb(II)	Ni(II)	Cd(II)
Langmuir	q_m (mg g^{-1})	73.52	43	44.16	30.39	20.27	109.72
$q_e = \frac{q_m b C_e}{(1+bC_e)}$	b (L mg^{-1})	0.454	0.025	0.119	0.384	0.0063	0.0073
	R^2	0.967	0.985	0.997	0.9032	0.9489	0.9765
Freundlich	K	20.33	1.615	6.736	10.86	0.194	0.947
$q_e = KC_e^{1/n}$	n	2.084	1.39	1.937	3.247	1.21	1.115
	R^2	0.914	0.974	0.9837	0.9885	0.9495	0.9823

$$\Delta G° = -RT \ln K_c \quad (11)$$

$$K_c = \frac{C_{ad}}{C_e} \quad (12)$$

where R is the gas constant (8.314 kJ K^{-1} mol^{-1}), T is the absolute temperature (K), K_c is the equilibrium constant, C_{ad} is the amount of metal adsorbed on the biosorbent or the nanosorbent per liter of the solution at equilibrium (mg L^{-1}), and C_e is the equilibrium concentration of the metal in the solution (mg L^{-1}). The change of enthalpy ($\Delta H°$) and entropy ($\Delta S°$) can be obtained from the slope and intercept of the Eq. (13) of $\Delta G°$ vs. T [42]:

$$\Delta G° = \Delta H° - T\Delta S° \quad (13)$$

where $\Delta H°$ is the enthalpy change (kJ mol^{-1}) and $\Delta S°$ is the entropy change (kJ mol^{-1} K^{-1}). Values of the standard Gibbs free energy for the adsorption process gained from Eq. (11) are listed in Tables 4 and 5 for both adsorbents. The negative value of $\Delta G°$ increased with an increase in temperature, suggesting that a better adsorption is actually at lower temperatures.

The standard enthalpy and entropy changes of adsorption were determined from Eq. (13). The negative values of $\Delta H°$ imply an exothermic nature of adsorption. Additionally, the positive values of $\Delta S°$ confirmed the decreased randomness at the solid-solute interface during the adsorption process, which shows the solution system trends toward instability when the adsorption of metals on the surface of both adsorbents occurred.

3.5. Effect of ion competition on nanosorption

Fig. 6 illustrates that advanced removal adsorption for the lead was achieved using a low dose of anaerobic biomass and more rapid affinity of lead towards the nanoparticles compared to other metal ions revealing the presence of various electrical attractions between cation lead metal and negative adsorption functional sites. Additionally, lead ions possess the smallest hydration radius, while nickel possesses the largest. This property causes lead ions highest to be favored by the biosorbent. This corresponds with the conception that ions which have a smaller hydration radius are desirably gathered at the interface [38]. Hydration energy plunges when the radius of metal ions in the solution increases [43]. Furthermore, lead nitrate salt is less

Table 4
Thermodynamic constants of adsorption obtained for Pb(II), Ni(II) and Cd(II) ions biosorption onto dead anaerobic biomass

Metal	Temperature (K)	$\Delta G°$ (kJ mol^{-1})	$\Delta H°$ (kJ mo1^{-1})	$\Delta S°$ (kJ mol^{-1} k^{-1})	R^2
Pb(II)	293	–12.10	–30.719	–0.0635	0.9973
	303	–11.48			
	318	–10.60			
	328	–9.84			
Ni(II)	293	–3.98	–15.023	–0.0376	0.9199
	303	–3.58			
	318	–3.22			
	328	–2.58			
Cd(II)	293	–8.57	–26.429	–0.0611	0.9634
	303	–7.69			
	318	–7.37			
	328	–6.18			

Table 5
Thermodynamic constants of adsorption obtained for Pb(II), Ni(II) and Cd(II) ions biosorption onto synthesized Fe_3O_4.

Metal	Temperature (K)	$\Delta G°$ (kJ mol^{-1})	$\Delta H°$ (kJ mo1^{-1})	$\Delta S°$ (kJ mol^{-1} k^{-1})	R^2
Pb(II)	293	–14.905	–76.863	0.2103	0.9685
	303	–13.856			
	318	–9.380			
	328	–8.109			
Ni(II)	293	1.397	–11.656	0.0443	0.9898
	303	1.683			
	318	2.413			
	328	2.919			
Cd(II)	293	–0.405	–8.0781	0.0261	0.9966
	303	–0.184			
	318	0.206			
	328	0.509			

soluble in water than nickel and cadmium salts. Therefore, an elevated adsorption rate on the surface of biomass can be achieved with higher molecular weights of adsorbate [44]. Hence, the sequence of the molecular weights for used pollutant salts is $Pb(NO_3)_2 > Cd(NO_3)_2 > Ni(NO_3)_3{\cdot}6H_2O$.

3.6. Kinetic process results

The optimum mass of dried dead anaerobic biomass (W_A) required to achieve 95% removal performance for a liter of metal solution (C_0 = 40 mg L^{-1} at 20°C) with final equilibrium concentration of C/C_0 = 0.05 was 1, 17.78 and 4.54 g for lead, nickel and cadmium respectively, determined through isothermal and balance equations for each solute according to the formula below [45]:

$$W_A = \frac{V_L\left(C_0 - C_e\right)}{q_e} = \frac{V_L\left(C_0 - C_e\right)}{\left[\frac{q_m b\, C_e}{1 + bC_e}\right]} \tag{14}$$

The optimum kinetic agitation speed was 400 rpm. Depending on the type of dead anaerobic biosorbent added to the metal solutions, the concentration decay curves of solutes are shown in Fig. 7 for the three metal ions at different agitation speeds. Table 6 and Fig. 8 demonstrate the parameter results and relationship of each kinetic model. Furthermore, the slope resulting from second-order kinetic model revealed better compliance compared to other models, the correlation coefficient was greater than 0.99 with a biosorption uptake equal to 37.89, 2.125 and 8.344 mg g^{-1} for lead, nickel and cadmium ions, respectively.

3.7. FTIR detection

Fig. 9 demonstrates the FTIR spectroscopic analysis for both adsorbents. The figure reveals four strong groups for biomass at 3,413–2,514 cm^{-1}, which denotes to (–OH) hydroxyl band. The peaks between 1,680–1,457 cm^{-1} represent carbonyl (–C=O) stretching vibration of the carboxyl groups. Peaks extending from 1,045 to 805 cm^{-1} are usually explained by (C–O) stretching vibration in carbonyl

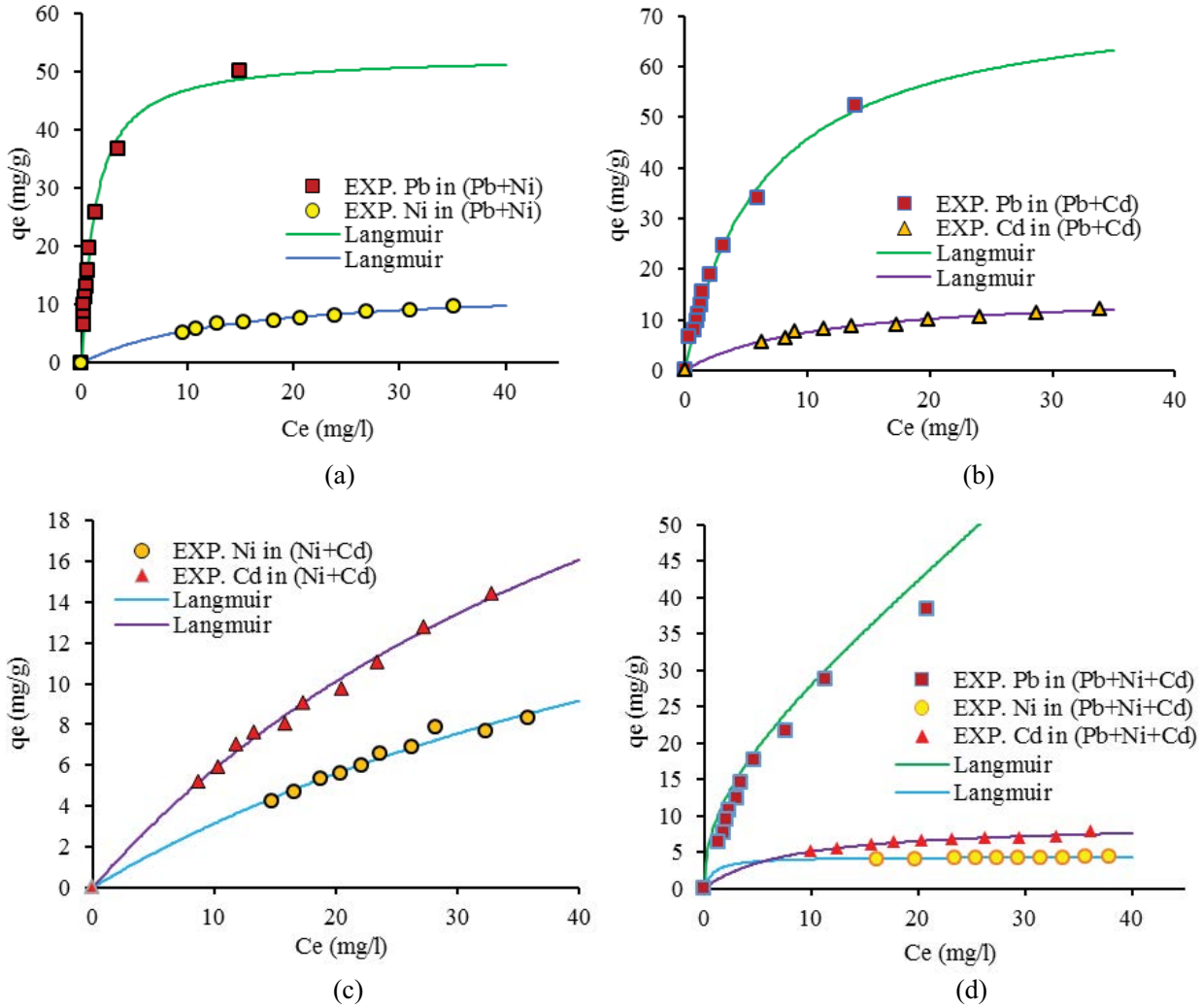

Fig. 6. Isothermal adsorption for the three metal ions onto dead anaerobic biomass in binary and ternary systems, C_0 [Pb, Ni, Cd] = 40 mg L^{-1}, pH = 4.

and alcohols. The results also imply that Pb(II), Ni(II) and Cd(II) ions are adsorbed or complexed by H and O atoms of hydroxyl and carboxylic bonds, which moved the spectra forward to a lower frequency. These movements are ascribed to the changes in counter ions associated with carboxylate and hydroxylate anions, suggesting that carboxyl and hydroxyl acidic groups are predominant contributors in the metal uptake [46]. The results also reveal that biosorption of Pb(II) leads to greater peaks and troughs due to its great affinity for biomass compared to other solute metals. The bands of functional groups shifted to a lower frequency with totals of 143, 52, and 93 for biomass loaded with Pb(II), Ni(II) and Cd(II), respectively. Consequently, the heavy metal biosorption order by way of complexation on the surface of biomass is as follows:

Pb(II) > Cd(II) > Ni(II).

With reference to Fe_3O_4 nanoparticles, FTIR analysis detected only two strong peak bands 3,394 and 1,638 cm^{-1} responsible for attracting metal ions in the bulk solution to be adsorbed on the surface of nanoparticles. The bands belonged to (–OH) hydroxyl and carbonyl (–C=O) group, respectively. Owing to the small size of nanosorbent particles, unlike biomass, no porosity existed on their external surface. Therefore, the biomass demonstrates greater feasibility and capability to adsorb solute metals from bulk solutions, compared with Fe_3O_4 nanosorbent.

3.8. Continuous process result

In the column study, the pressure drop readings from the piezometer for both anaerobic biomass bed at different flowrates and static bed height inside the column were, quite small. Minimum fluidization velocity (U_{mf}) was evaluated as 4.193 mm s^{-1}, leading to motion and consequently making the uniform mass transfer of contaminants from bulk liquids to the surface of biomass adsorbent, whilst at the same time avoiding simultaneously the formation of dead zones. Fig. 10 reveals that breakpoint time to reach equilibrium for the lead, nickel and cadmium ions was reduced by having small bed heights inside the column due to fewer available

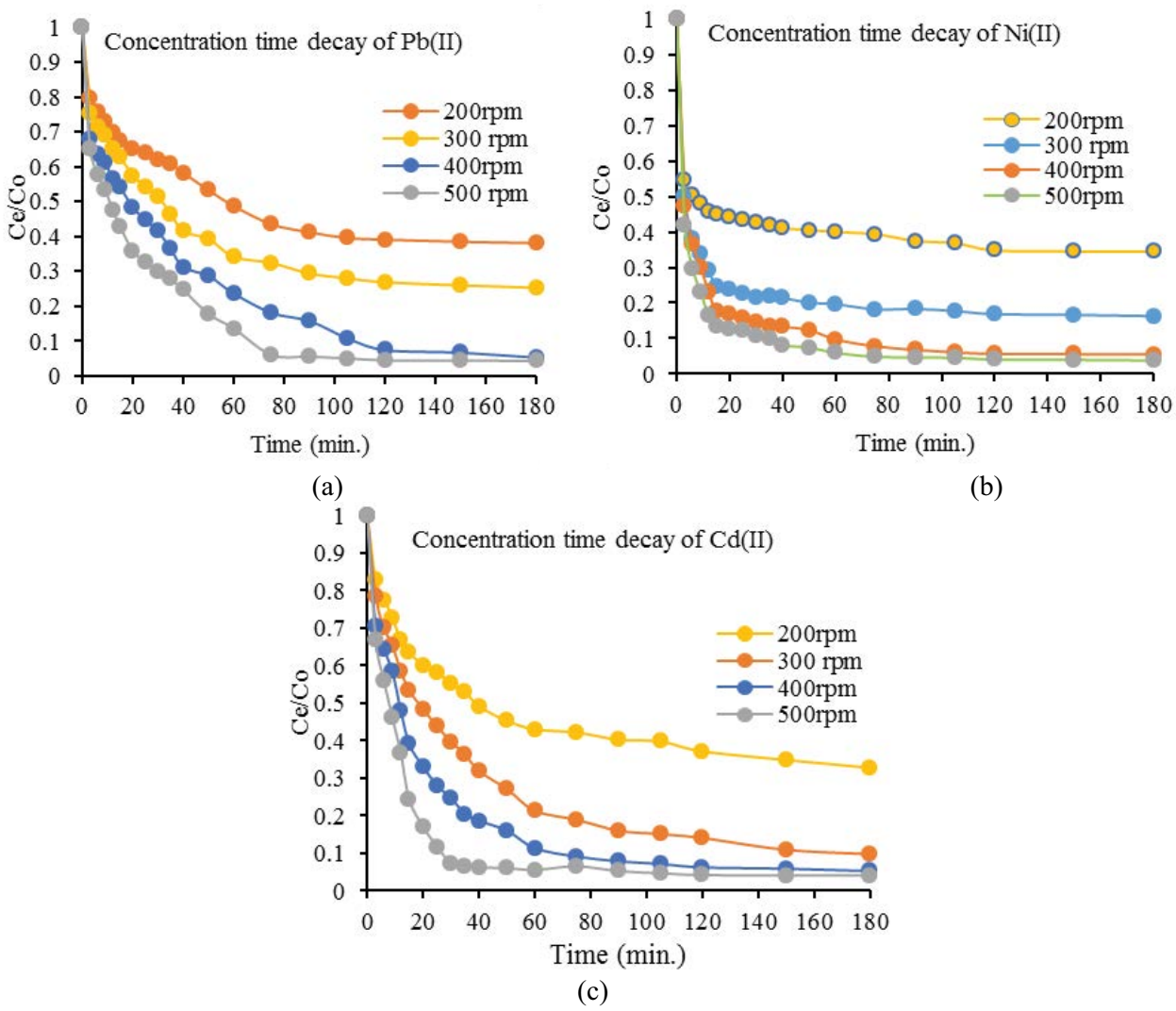

Fig. 7. Concentration-time decay curves for Pb(II), Ni(II) and Cd(II) onto anaerobic biomass in kinetic process at different agitation speeds, C_0 = 40 mg L^{-1} and pH = 4.

Table 6
Kinetic model parameters for Pb(II), Ni(II) and Cd(II) ions biosorption onto dead anaerobic biomass

Model	Parameters	Pb(II)	Ni(II)	Cd(II)
Intraparticle diffusion	C (mg g^{-1})	7.871	1.142	2.51
	K_{id} (mg g^{-1} $min^{-0.5}$)	2.65	0.1013	0.568
	R^2	0.9304	0.559	0.797
Pseudo-first-order	q_e (mg g^{-1})	30.8	5.32	0.908
	k_1 (min^{-1})	0.0261	0.0336	0.043
	R^2	0.9788	0.9791	0.9631
Pseudo-second-order	q_e (mg g^{-1})	37.89	2.125	8.344
	k_2 (mg g^{-1} min^{-1})	0.134	1.36 E-03	0.011
	R^2	0.9998	0.9993	0.9934
Elovich	a (mg g^{-1} min^{-1})	8.021	40.47	2.75
	b (g mg^{-1})	0.1392	4.6425	0.629
	R^2	0.9657	0.9056	0.9511

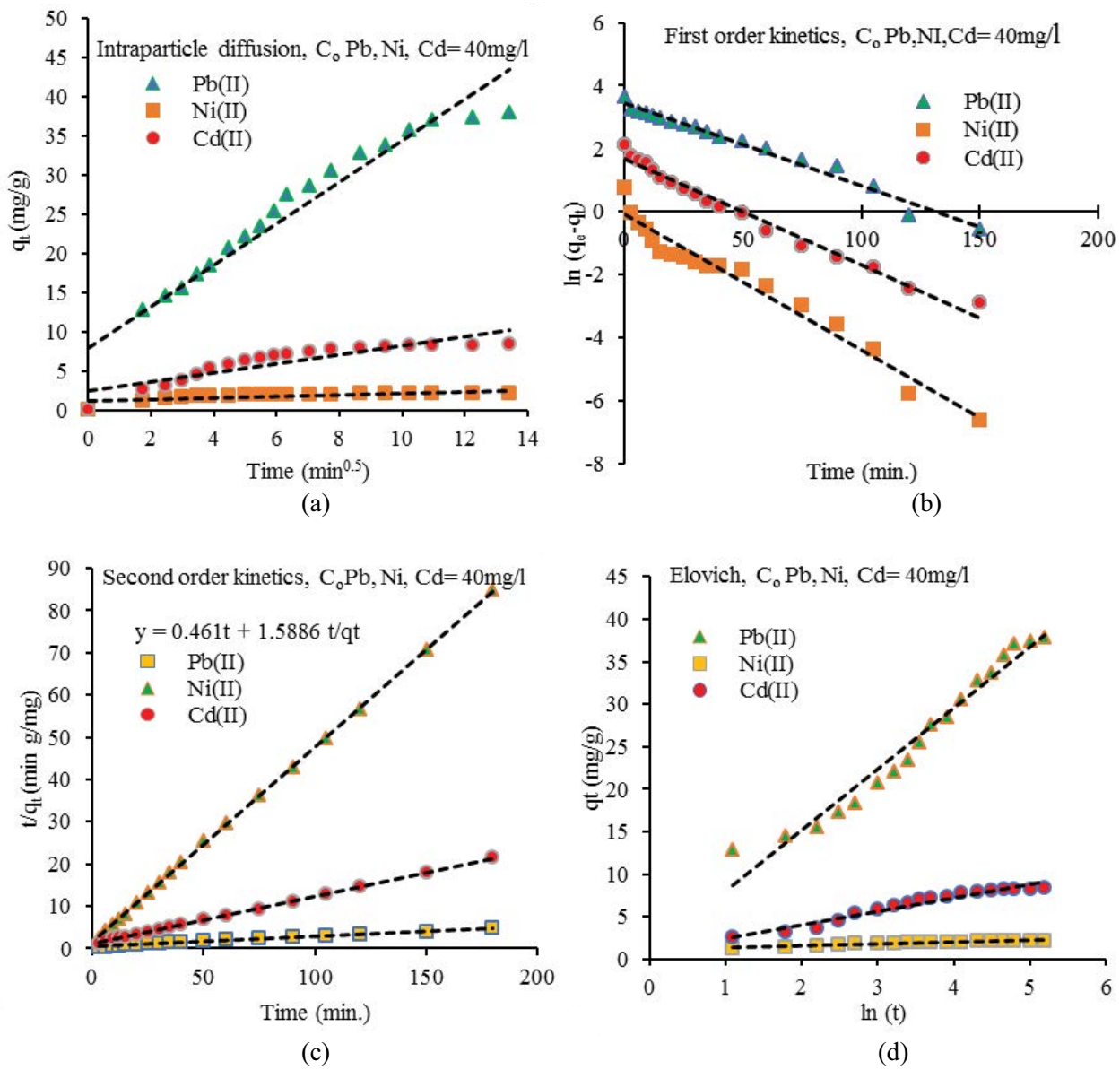

Fig. 8. Different kinetic models for biosorption of Pb(II), Ni(II) and Cd(II) onto dead anaerobic biomass.

adsorption sites. This result is compliant with that obtained by Ahmad and Hameed [47] and Futalan et al. [48]. Fig. 10 also shows that lead ions have the largest breakthrough time and least steepness compared to nickel and cadmium ions. Fig. 11 indicates the influence of flow variation through the column. Flowrate modification of metal solutions from 1.1 to 1.4 U_{mf} through bed particles causing inadequate contact time between metal pollutants and biosorbent, less uptake of metal ions, noticeable depletion in biosorption capacity, high steepness of breakthrough curves and perceptible reduction in breakpoint due to the presence of high intra-particle resistance [49]. However, the thickness of boundary layer film that surrounds the biomass particles can be reduced. This causes a reduction in the resistance of mass transfer of solute pollutants to be adsorbed onto the surface of the biomass. In high flow operation (1.4 U_{mf}) and 75 g of biomass inside the column, the break time to reach equilibrium for the lead, nickel and cadmium ions respectively was 110, 80 and 100 min compared with 120, 90 and 110 min for 1.1 U_{mf} flow. The patterns of the three metal breakthrough curves depended on their steepness which decreased in the order of Pb(II) > Cd(II) > Ni(II) and the experimental breakthrough data of metal ions were fitted well with the predicted data obtained by applying artificial neural network in IBM SPSS software version-19.

4. Conclusions

Removal of metal solutes by waste biosorbent and Fe_3O_4 nanosorbent are strongly affected by various factors including pH value, efficient contact time and molecular weight, size of adsorbate molecules, initial heavy metal

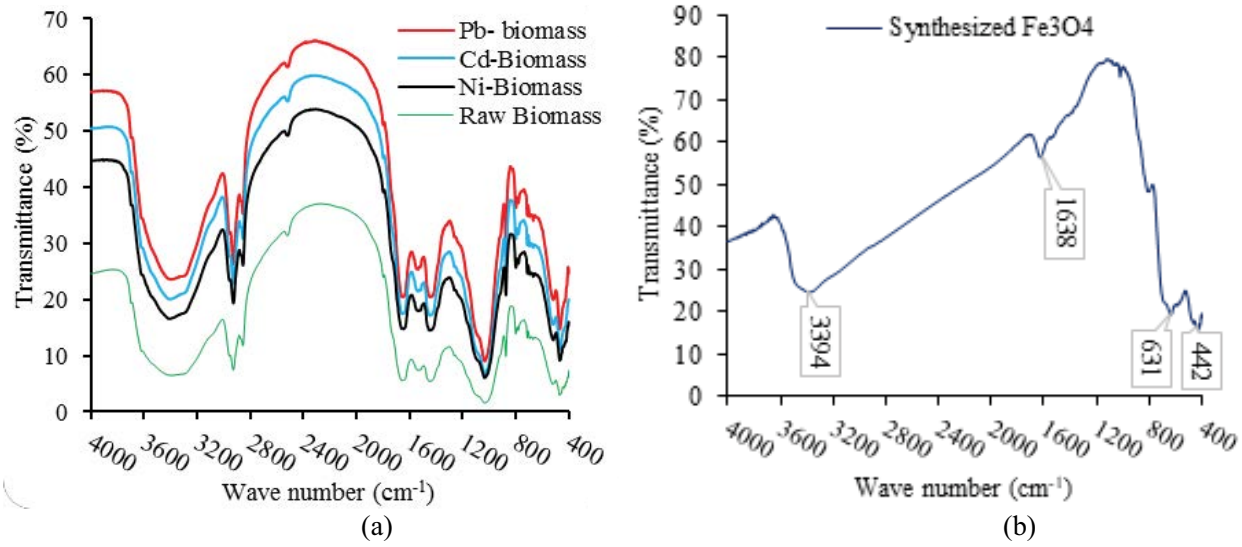

Fig. 9. FTIR spectra for (a) Raw dead anaerobic biomass before and after loaded with 40 mg L^{-1} of the metals and (b) Raw synthesized Fe_3O_4 nanoparticles.

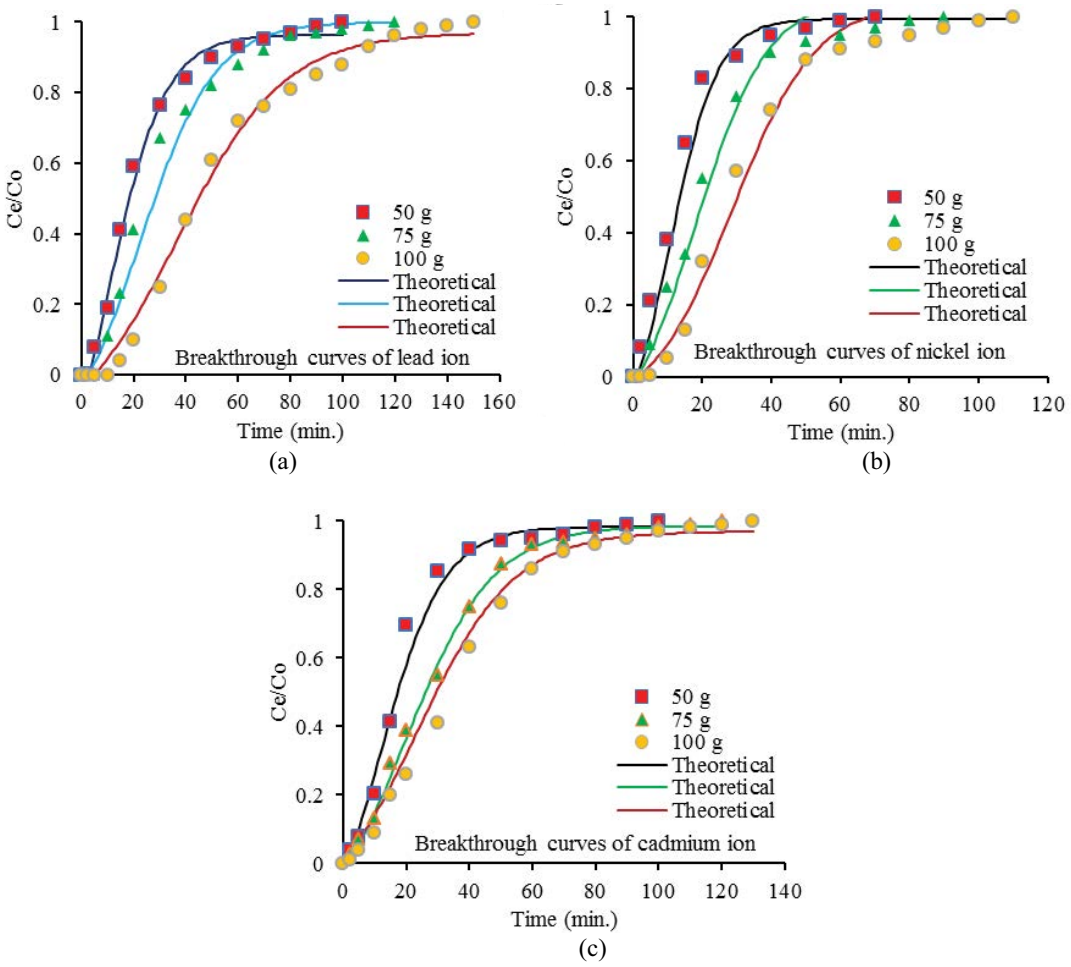

Fig. 10. Experimental data and theoretical breakthrough curves for biosorption of metal ions at different bed weights, C_0 = 40 mg L^{-1}, U = 1.1 U_{mf}, dp = 0.5–0.9 mm diameter.

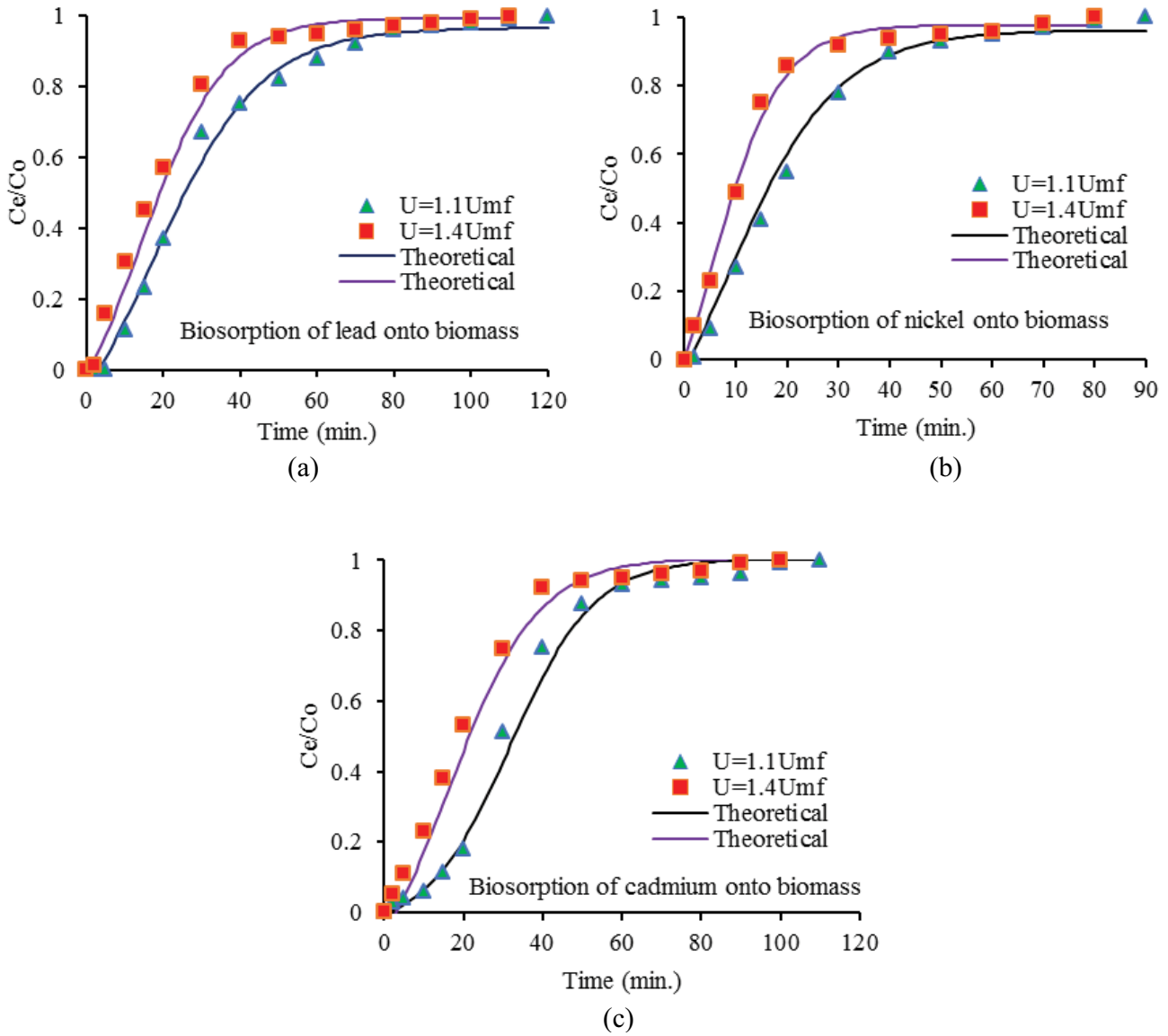

Fig. 11. Experimental data and theoretical breakthrough curves for biosorption of metal ions at different fluid velocities, C_0 = 40 mg L^{-1}, w = 75 g, 6.1 cm bed height, dp = 0.5–0.9 mm diameter.

ion concentration and adsorbent quantity. The transition of lead metal ions from bulk liquids in the aqueous solution to the surface of both adsorbents faces lower resistance than both nickel and cadmium. The performance and adsorption capability of the anaerobic biosorbent is much higher than synthesized Fe_3O_4 nanosorbent. The presence of more negative and energetic functional sites on the surface of biomass, different pore sizes in the structure of the biosorbent and having varying active compositions (detected by FTIR and XRF) are the main reasons why the anaerobic biosorbent performs better in terms of adsorbing metals and demonstrating higher removal rates compared to synthesized Fe_3O_4 nanosorbent. Therefore, the biomass is not only more economically feasible to operate, but also environmentally helpful in reducing the amount of sludge transferred to disposal site after capturing heavy metals of Pb(II), Ni(II), and Cd(II) and using as organic fertilizer in the agricultural fields. The sludge biomass in the soil is subjected to decompose through the action of soil microorganisms to provide necessary nutrients for plant growth. Furthermore, the adsorbed heavy metals of Pb(II), Ni(II), and Cd(II) in the sludge can be absorbed by the roots of the plants through phytoremediation process and accumulated in their shoots. Periodically, these plants are harvested for metal recovery.

Acknowledgments

The authors are thankful to the Kurdistan Institute for Strategic Studies and Scientific Research in Sulaymaniyah, Iraq for their support and analytical test services. Also, financial support from the University of Sulaimani was most helpful in achieving this work.

References

[1] J.C. Akan, M.T. Abbagambo, Z.M. Chellube, F.I. Abdulrahman, Assessment of Pollutants in Water and Sediment Samples in Lake Chad, Baga, North Eastern Nigeria, J. Environ. Prot., 3 (2012) 1428–1441.

[2] J.A. Akankali, E.I. Elenwo, Sources of marine pollution on nigerian coastal resources: an overview, Open J. Mar. Sci., 5 (2015) 226–236.

[3] C.K. Takahashi, A. Turner, G.E. Millward, G.A. Glegg, Persistence and metallic composition of paint particles in sediments from a tidal inlet, Mar. Pollut. Bull., 64 (2012) 133–137.

[4] M.N. Sahmoune, K. Louhab, A. Boukhiar, Biosorption of Cr (III) from aqueous solutions using bacterium biomass *Streptomyces rimosus*, Int. J. Environ. Res., 3 (2009) 229–238.

[5] G.F. de Mattos, C. Costa, F. Savio, M. Alonso, G.L. Nicolson, Lead poisoning: acute exposure of the heart to lead ions promotes changes in cardiac function and Cav1.2 ion channels, Biophys. Rev., 9 (2017) 807–825.

[6] P. Harasim, T. Filipek, Nickel in the environment, J. Elem., 20 (2015) 525–534.

[7] S. Mbarek, T. Saidi, H.B. Mansour, M.P. Stéphane, W. Rostene, R.B. Chaouacha-Chekir, Effect of cadmium on water metabolism regulation by *Meriones shawi* (Rodentia, Muridae), Environ. Eng. Sci., 28 (2011) 237–248.

[8] J. Wilkinson, P.S. Hooda, J. Barker, S. Barton, J. Swinden, Occurrence, fate and transformation of emerging contaminants in water: an overarching review of the field, Environ. Pollut., 231 (2017) 954–970.

[9] N.H. Tran, M. Reinhard, K.Y.-H. Gin, Occurrence and fate of emerging contaminants in municipal wastewater treatment plants from different geographical regions-a review, Water Res., 133 (2018) 182–207.

[10] D. Mohan, A. Sarswat, Y.S. Ok, C.U. Pittman Jr., Organic and inorganic contaminants removal from water with biochar, a renewable, low cost and sustainable adsorbent – a critical review, Bioresour. Technol., 160 (2014) 191–202.

[11] M. Asgher, Q. Yasmeen, H.M.N. Iqbal, Enhanced decolorization of solar brilliant red 80 textile dye by an indigenous white rot fungus *Schizophyllum commune* IBL-06, Saudi J. Biol. Sci., 20 (2013) 347–352.

[12] V. Sharma, A. Sharma, Nanotechnology: an emerging future trend in wastewater treatment with its innovative products and processes, Int. J. Enhance Res. Sci. Technol. Eng., 1 (2012) 1–8.

[13] J. Shen, G. Huang, C. An, X. Xin, C. Huang, S. Rosendahl, Removal of Tetrabromobisphenol A by adsorption on pinecone-derived activated charcoals: synchrotron FTIR, kinetics and surface functionality analyses, Bioresour. Technol., 247 (2018) 812–820.

[14] G. Ersan, O.G. Apul, F. Perreault, T. Karanfil, Adsorption of organic contaminants by graphene nanosheets: a review, Water Res., 126 (2017) 385–398.

[15] D.U. Handojo, S.M. Razman, Adsorption of heavy metals from water and waste water using low cost adsorbents from agricultural by-products, Asian J. Water Environ. Pollut., 6 (2009) 73–80.

[16] P. Ziarati, F.M. Mohammad-Makki, M. Moslehishad, Novel adsorption method for contaminated water by wild endemic almond: *Amygdalus Scopar*, Biosci. Biotechnol. Res. Asia, 13 (2016) 147–153.

[17] A. Pourzare, P. Ziarati, Z. Mousavi, A.R. Faraji, Removing cadmium and nickel contents in basil cultivated in pharmaceutical effluent by chamomile (*Matricaria chamomilla* L.) tea residue, J. Sci. Discovery, 1 (2017).

[18] A.S. Ayangbenro, O.O. Babalola, New strategy for heavy metal polluted environments, a review of microbial biosorbents, Int. J. Environ. Res. Public Health, 14 (2017) 94.

[19] T. Dokulilová, T. Vítěz, J. Chovanec, R. Rous, M. Vítězová, I. Kushkevych, Primary and activated sludge biogas production: effect of temperature, 66 (2018) 23–28.

[20] R. Taman, M.E. Ossman, M.S. Mansour, H.A. Farag, Metal oxide nanoparticles as an adsorbent for removal of heavy metals, J. Adv. Chem. Eng., 5 (2015) 1–11.

[21] W. Wu, Z. Wu, T. Yu, C. Jiang, W.S. Kim, Recent progress on magnetic iron oxide nanoparticles: synthesis, surface functional strategies and biomedical applications, Sci. Technol. Adv. Mater., 16 (2015) 1–44.

[22] M. Sandeep, V. Kumar, Magnetic nanoparticles-based biomedical and bioanalytical applications, Nanotechnology, 4 (2013) 1–2.

[23] Federation W.E., American Public Health Association, Standard Methods for the Examination of Water and Wastewater, American Public Health Association (APHA), Washington, D.C., USA, 2005.

[24] A.P. Mathews, I. Zayas, Particle size and shape effects on adsorption rate parameters, Environ. Eng., 115 (1989) 41–55.

[25] N.D. Kandpal, N. Sah, R. Loshali, R. Joshi, J. Prasad, Co-precipitation method of synthesis and characterization of iron oxide nanoparticles, J. Sci. Ind. Res., 73 (2014) 87–90.

[26] Y.F. Lam, L.Y. Lee, S.J. Chua, S.S. Lim, S. Gan, Insights into the equilibrium, kinetic and thermodynamics of nickel removal by environmentally friendly Lansium domesticum peel adsorbent, Ecotoxicol. Environ. Saf., 127 (2016) 61–70.

[27] L. Anah, N. Astrini, Influence of pH on Cr (VI) ions removal from aqueous solutions using carboxymethyl cellulose-based hydrogel as adsorbent, IOP Conf. Ser.: Earth Environ. Sci, 60 (2017) 012010.

[28] A.M. Mahmoud, F.A. Ibrahim, S.A. Shaban, N.A. Youssef, Adsorption of heavy metal ion from aqueous solution by nickel oxide nano catalyst prepared by different methods, Egypt J. Petrol., 24 (2015) 27–35.

[29] K. Vijayaraghavan, Y.S. Yun, Bacterial biosorbents and biosorption, Biotechnol. Adv., 26 (2008) 266–291.

[30] S.K. Lagergren, About the theory of so-called adsorption of soluble substances, Vet. Hand., 24 (1898) 1–39.

[31] A.M. Farhan, N.M. Salem, A.L. Ahmad, A.M. Awwad, Kinetic equilibrium and thermodynamic studies of the biosorption of heavy metals by *Ceratonia siliqua* bark, Am J. Chem., 2 (2012) 335–342.

[32] H. Ys, L. Egghe, A.F.J. van Raan, W. Glanzel, H. Moed, W. Glanzel, K. Borner, Citation review of Lagergren kinetic rate equation on adsorption reactions, Sci. Metrics, 59 (2004) 171–177.

[33] O. Abdi, M. Kazemia, A review study of biosorption of heavy metals and comparison between different biosorbents, J. Mater. Environ. Sci., 6 (2015) 1386–1399.

[34] N. Singh, S.K. Gupta, Adsorption of heavy metals: a review, Int. J. Environ. Res. Dev., 5 (2016) 2267–2281.

[35] R. Ghasemi-Fasaei, A. Ronaghi, E. Farrokhnejad, Comparative study of metal micronutrients releases from two calcareous soils, Arch. Agron. Soil Sci., 58 (2012) 1171–1178.

[36] Y. Yadav, R. Gothalwal, R.K. Tenguriya, Management of heavy metal pollution by using bacterial biomass, Int. J. Biotechnol. Trends Technol., 8 (2018) 1–12.

[37] C. Quintelas, B. Fernandes, J. Castro, H. Figueiredo, T. Tavares, Biosorption of Cr(VI) by three different bacterial species supported on granular activated carbon—a comparative study, J. Hazard. Mater., 153 (2008) 799–809.

[38] Y. Chen, W. Zhao, H. Wang, X. Meng, L. Zhang, A novel polyamine-type starch/glycidyl methacrylate copolymer for adsorption of Pb(II), Cu(II), Cd(II) and Cr(III) ions from aqueous solutions, R. Soc. Open Sci., 5 (2018) 180281.

[39] M. Ji, X. Su, Y. Zhao, W. Qi, Y. Wang, G. Chen, Z. Zhang, Effective adsorption of Cr (VI) on mesoporous Fe-functionalized Akadama clay: optimization, selectivity, and mechanism, Appl. Surf. Sci., 344 (2015) 128–136.

[40] S.E. Ebrahim, A.H. Sulaymon, H. Saad Alhares, Competitive removal of Cu^{+2}, Cd^{+2}, Zn^{+2}, and Ni^{+2} ions onto iron oxide nanoparticles from wastewater, Desal. Wat. Treat., 57 (2015) 20915–20929.

[41] A. Kakaei, M. Kazemeini, Removal of Cd (II) in water samples using modified magnetic iron oxide nanoparticle, Iran. J. Toxicol., 10 (2016) 9–14.

[42] G. Blázquez, M.A. Martín-Lara, G. Tenorio, M. Calero, Batch biosorption of lead (II) from aqueous solutions by olive tree pruning waste: equilibrium, kinetics and thermodynamic study. Chem. Eng. J., 168 (2011) 170–177.

[43] R. Mahmudov, C.P. Huang, Selective adsorption of oxyanions on activated carbon exemplified by Filtrasorb 400 (F400), Sep. Purif. Technol., 77 (2011) 294–300.
[44] K. Al-Essa, F. Khalili, Heavy metals adsorption from aqueous solutions onto unmodified and modified jordanian kaolinite clay: batch and column techniques, Am. J. Appl. Chem., 6 (2018) 25–34.
[45] K.W. Ahmed, Experimental and Modeling for the Removal of Multi-pollutants by Adsorption, Ph.D. Thesis, College of Engineering, University of Baghdad, Baghdad, 2006.
[46] S. Srivastava, P. Singh, R. Bhagat, Application of bacterial biomass as a potential metal indicator, Curr. Sci., 89 (2005) 1248–1251.
[47] A. Ahmad, B. Hameed, Fixed-bed adsorption of reactive azo dye onto granular activated carbon prepared from waste, J. Hazard. Mater., 175 (2010) 298–303.
[48] C.M. Futalan, C.C. Kan, M.L. Dalida, C. Pascua, M.W. Wan, Fixed-bed column studies on the removal of copper using chitosan immobilized on bentonite, Carbohydr. Polym., 83 (2011) 697–704.
[49] S. Singha, U. Sarkar, Analysis of the dynamic column using semi-empirical models: case studies with removal of hexavalent chromium from effluent wastewater, Korean J. Chem. Eng., 32 (2015) 20–29.